Evaluation of tropical cloud and precipitation simulations of CAM3 using CloudSat and CALIPSO data

Y. Zhang[1], S. A. Klein[1], J. Boyle[1], and G. G. Mace[2]

1. Lawrence Livermore National Laboratory, Livermore, California

2. Department of Meteorology, University of Utah, Salt Lake City, Utah

Submitted to the Journal of Geophysical Research - Atmospheres

Abstract

CloudSat and CALIPSO satellite observations provide the first global measurements of the vertical structure of clouds and precipitation, and are used to examine the representation of tropical clouds and precipitation in the Community Atmosphere Model Version 3 (CAM3). Mesoscale patterns of clouds and precipitation are characterized by the joint histograms of atmospheric pressure and signal strength, and a revised clustering method is used to sort the mesoscale patterns into principal cloud regimes. A simulator package utilizing a model-to-satellite approach facilitates comparison of model simulations to observations.

Results from weather forecasts performed with CAM3 suggest that the model underestimates the occurrence of low and mid-level clouds, but overestimates that of high clouds. CAM3 overestimates the frequency of occurrence of the deep convection with heavy precipitation regime, but underestimates the horizontal extent of clouds and precipitation when the regime occurs. This suggests that the model overestimates convective precipitation and underestimates stratiform precipitation. Tropical cloud regimes are also evaluated in a different version of the model, CAM3.5, which uses a highly entraining plume in the parameterization of deep convection. The frequency of occurrence of different regimes from CAM3.5 forecasts compares more favorably to observations with a reduced incidence of the cirrus and deep convection with heavy precipitation regimes and an increased incidence of the low clouds with precipitation and congestus regimes. Despite these improvements, model clouds and precipitation remain overly reflective in most cloud regimes, and low- and mid-level clouds precipitate too heavily. By stratifying the frequency of occurrence of cloud regimes according to the

65 monthly mean 500 hPa vertical pressure velocity, the association between tropical cloud
66 regimes and monthly mean vertical motion is explored.
67

1. Introduction

Although Global Climate Models (GCMs) are the primary tools to predict climate change, large uncertainties remain in projections of future climate after more than 30 years of GCM development (Houghton et al., 2001; Randall et al., 2007). The different representations of clouds and their feedback processes in GCMs have been identified as the major source of differences in model climate sensitivities (Cess et al. 1990; Soden et al. 2004; Zhang et al. 2005). These differences arise because contemporary GCMs cannot resolve clouds and highly simplified parameterizations are used to represent the interactions between clouds and radiation and the large-scale environment resolved by GCMs. It has been pointed out that improved present-day cloud simulations are needed to reduce the uncertainties in predicting future climate (Bony et al. 2006; Williams and Tselioudis, 2007). Widely collected observations are required to assess model performance and provide valuable information for the development of new parameterizations. However, the evaluation of GCM cloud simulations has long been hampered by the lack of suitable observations.

Field programs with intensive observations are not sufficient to solve the parameterization problem, because it is unlikely that a few cases will be representative enough. Traditional methods to obtain global perspective, such as the International Satellite Cloud Climatology Project (ISCCP; Rossow and Schiffer, 1999) and the Earth Radiation Budget Experiment (ERBE; Wielicki et al. 1996) rely on radiances observed by passive sensors on satellites. But because these radiances depend on the integrated effect of properties of the whole atmospheric column, they provide little information of the vertical structure of cloud fields. The lack of vertical structure information prevents an understanding of the hydrologic cycle and the modulation by clouds of the vertical

93 distribution of radiative heating rates; it also hinders the evaluation of GCM cloud
94 simulations. Launched in April 2006, the CloudSat and CALIPSO satellites, flying in the
95 A-Train constellation (Stephens et al. 2002), provide the first global survey of the vertical
96 distribution of cloud condensate and precipitation. The Cloud Profiling Radar (CPR) on
97 CloudSat (Im et al., 2006) is the first spaceborne millimeter-wavelength radar capable of
98 penetrating optically thick hydrometeor layers. The CALIPSO satellite carries a lidar
99 system (Winker et al., 2007) as its primary payload capable of detecting optically thin
100 clouds. The combined information from the two instruments is able to accurately
101 characterize the vertical as well as horizontal structure of hydrometeor layers (Mace et al.
102 2008). The only clouds missed by the combined dataset are low-level clouds with
103 reflectivity less than the detection threshold of the radar that are also beneath clouds
104 which completely attenuate the lidar pulse (Mace et al. 2008).

105 In this study, CloudSat and CALIPSO data are used to evaluate cloud and
106 precipitation simulations from CAM3, a major United States climate model. Traditional
107 methods of GCM evaluation use maps of large spatial and temporal means of cloud
108 variables from both models and observations. However, this method cannot provide an
109 effective constraint on cloud simulations and cannot assess cloud radiative feedback due
110 to compensating errors (Norris and Weaver, 2001; Williams et al., 2005). Another
111 popular method is to investigate relationships between clouds and other atmospheric
112 parameters using compositing techniques (Ringer and Allan, 2004). Atmospheric
113 parameters, such as 500-hPa vertical velocity, sea surface temperature, and lower
114 tropospheric stability (Bony et al., 2004; Williams et al. 2006), have been used in order to
115 document the relationships between clouds and the parameters that are thought to affect
116 their evolution. However, it is difficult to identify a small set of key atmospheric

parameters (Williams et al., 2003; Bony et al., 2004), and there is a lack of reliable data for some atmospheric parameters. In this study, the cluster analysis method is used to objectively identify cloud regimes based on cloud observations alone without any knowledge of other meteorological parameters. By looking for distinctive cloud mesoscale patterns in ISCCP data, this method has been widely used to characterize cloud regimes and evaluate model simulations in recent years (Jakob and Tselioudis, 2003; Rossow et al., 2005; Williams and Tselioudis, 2007; Chen and Del Genio, 2008). This method has also been used to evaluate precipitation regimes from Tropical Rainfall Measurement Mission (TRMM) precipitation radar data (Boccippio et al., 2005) and cloud regimes in CloudSat data (Zhang et al., 2007; hereafter Zhang07). This is the first study to use the cluster analysis method on the combined data from CloudSat and CALIPSO to evaluate cloud and precipitation simulations of a climate model.

The paper is organized as follows. In the next section, observational data, model simulations, and the cluster analysis method are briefly described. The simulator package that converts model output to observed variables is introduced in section 3, and cloud regimes from observational data are described in section 4. In section 5, model simulations are evaluated within the clustering framework, and changes resulting from the addition of new parameterizations to the CAM are shown. A summary is provided in section 6.

2. Data and Methodology

2.1 Observations

The CloudSat and CALIPSO satellites are maintained in tight orbital configuration to facilitate merging of data streams. The orbit is sun-synchronous with the overpass occurring around 1:30 am/pm local time. The ground track repeats every 16 days, and the

orbital period is 99 minutes. The CPR on CloudSat is a 94-GHz nadir-pointing radar that records range-resolved profiles of backscattered power with a nominal footprint of 1.4 km across by 2.5 km along track. Due to the sensitivity of the radar to large particles, the CPR detects both clouds and precipitation. The estimated CPR minimum detectable signal is -30 dBZ, and contamination by surface reflection in the lowest 500m of the atmosphere renders the signal unusable for hydrometeor identification (Mace et al. 2007). Due to these limitations, CloudSat will miss some fraction of thin cirrus, mid-level liquid water clouds, and non-precipitating cumulus and stratocumulus clouds as well as all low-level clouds below 500m.

The two-wavelength (1064 nm and 532 nm) polarization lidar on CALIPSO provides high resolution vertical profiles of backscattered power from which clouds and aerosols may be identified. The lidar system, which has higher horizontal and vertical resolution than the CPR, has the capability to sense optically thin layers with optical depths of 0.01 or less (Winker et al. 2007), and other clouds such as non-precipitating stratocumulus whose reflectivity is below the detection threshold of the radar. On the other hand, the lidar quickly attenuates beyond optical depths of about 3 and cannot detect many clouds and precipitation identified by the radar (Zhang and Mace 2006; Mace et al. 2008). The CPR and the CALIPSO lidar complement each other in their capabilities to observe clouds.

In this study, two CloudSat standard data products are used to characterize cloud vertical structures. The first is the Level 2 GEOPROF product (Mace 2004; Mace et al. 2007) which identifies the occurrence of hydrometeors with a masking algorithm and provides the radar effective reflectivity factor, Z_e, expressed in dBZ($=10\log_{10}Z_e$). The masking algorithm is described in more detail by Marchand et al. (2008). The second is

166 the Level 2 GEOPROF-LIDAR product (Mace et al. 2008) which contains the estimates
167 of lidar-determined cloud fraction within CPR sample volumes. The lidar information is
168 from the CALIPSO Level 2 Vertical Feature Mask which reports the location of aerosol
169 and cloud types.

170 In this study, tropical (23.5˚S − 23.5˚N) observations for the period June-
171 September in 2006 are used. Although not shown here, data for the same months in 2007
172 confirm the robustness of the results. Following the approach in Zhang07, a sequence of
173 200 adjacent profiles of satellite data (approximately 2° of latitude) define an individual
174 cloud region from which joint histograms of atmospheric pressure and signal strength are
175 computed to characterize the mesoscale patterns of cloud and precipitation. The
176 histograms contain the relative frequency of occurrence (RFO) of clouds and
177 precipitation in categories of seven signal bins and seven pressure levels; a sample
178 histogram is shown in Figure 1. To construct the joint histograms, radar reflectivity above
179 -30 dBZ with CPR cloud mask greater than or equal to 20, which means clouds with low
180 chance of a false detection (Marchand et al., 2008), is binned into six categories with a
181 bin interval of 10 dBZ. A seventh bin at the left side of the diagram displays the RFO of
182 lidar detected clouds which are not detected by the radar because the reflectivity is less
183 than -30 dBZ, the minimum detectable signal of the radar. The reported RFO is the
184 percentage of observations within a given pressure bin that have the reported signal
185 strength. Thus, if all volumes within a given pressure range for a 2° region had cloud or
186 precipitation identified by either CloudSat or CALIPSO, then the sum of RFOs over all 7
187 signal bins in the given pressure range would be 100%. To facilitate comparison with
188 previous cluster studies using ISCCP data, the boundaries of the seven pressure bins
189 coincide with those used by ISCCP, and the conversion from altitude to pressure is

attained by use of analysis data provided by the European Center for Medium-range Weather Forecasts (ECMWF) in the ECMWF-AUX product released with CloudSat and CALIPSO data. The characteristic patterns of this joint histogram will be used in the cluster analysis technique to determine tropical cloud regimes. While these 200-profile snapshots are created sequentially, a sensitivity study, which uses another set of snapshots collected by taking a 100-profile step forward compared with the original set, shows that these 200-profile snapshots are able to independently represent the tropical cloud regimes.

2.2 CAM3 and model integrations

In this study, cloud and precipitation simulations of the Community Atmospheric Model version 3.1 (Collins et al., 2006) are examined. The version of CAM3.1 used in this study employs the finite volume dynamical core with horizontal resolution of 1.9º latitude by 2.5º longitude and 26 vertical levels. CAM 3.1 treats stratiform cloud microphysics based on the prognostic cloud water formulation of Rasch and Kristjansson (1998) with modifications made by Zhang et al. (2003). There are two parameterizations of moist convection in the model: a shallow depth mixing parameterization (Hack 1993) and a deep convection parameterization (Zhang and McFarlane, 1995) which convects whenever the convective available potential energy exceeds a small threshold of 70 J/kg.

In addition to CAM3.1, a later version of the model, CAM3.5, will also be evaluated. While there are numerous differences between the two versions, the key difference lies in two modifications to the parameterization of deep convection. The first modification is the inclusion of a parameterization of cumulus momentum transport (Richter and Rasch, 2008). The second modification uses a highly entraining (as opposed to undilute) plume to calculate available potential energy and prohibits convection when

there is no available potential energy for this entraining plume (Neale et al., 2008). As a result, deep convection will be suppressed if the troposphere is dry even if the convective available potential energy for an undilute plume exceeds 70 J/kg.

Although CAM is a climate model, we examine simulations of CAM performed in weather-forecast mode (Phillips et al., 2004) to better identify parameterization-related deficiencies in the simulation of clouds and precipitation. With a weather-forecasting approach, it is more likely that errors can be ascribed to the model parameterizations of moist processes, because the large-scale atmospheric state in the early periods of a forecast is relatively close to reality. In this study, a series of forecasts are performed which commence every day in the time period from June to September 2006. Forecasts are initialized from analyses of the National Center for Environmental Prediction (NCEP) and we examine model data from day-2 forecasts.

Considering the overpass time of the A-Train constellation, the model simulations at 1 am and pm local time are compared to observations. Tests show that the geographical distribution of the RFO of cloud regimes significantly changes if simulator output at other times is used while the joint histograms of atmospheric pressure and signal strength are still similar to those from model output at 1 am and 1pm local time. This reminds the reader that some of the geographical patterns shown below result from an incomplete sampling of the diurnal cycle by CloudSat and CALIPSO (Liu et al., 2008).

2.3 Clustering method

In this paper, the joint histograms of atmospheric pressure and signal strength are used to characterize the vertical distributions of hydrometeors. In Zhang07, characteristic patterns in these histograms of CloudSat data were identified using a K-means cluster algorithm (Anderberg, 1973). The algorithm determined the patterns from a vector that

238 consisted of the 42 independent elements of the joint histogram. A drawback of this
239 method is that information on the distance in pressure or signal strength between
240 elements is not considered and thus results may be sensitive to the discretization of the
241 histogram (Williams and Webb, 2008). As an alternative, clustering is performed using a
242 7 element vector that equivalently illustrates the vertical profiles of signal strength. This 7
243 element vector which we call the normalized mean dBZ index is computed from the joint
244 histogram of cloud patterns in the following manner. As depicted in the upper abscissa of
245 Figure 1 (c), a dBZ index integer for each bin of signal strength is assigned. For example,
246 if the radar reflectivity dBZ is between -20 and -10, the dBZ index is 3. Likewise if the
247 hydrometeor is detected by the lidar only, the dBZ index is set to 1. The normalized mean
248 dBZ index at each of the 7 pressure levels is computed as the sum of RFO_{cld}*dBZ_ind,
249 where RFO_{cld} is the relative occurrence frequency of a certain dBZ range/lidar bin in all
250 the cloudy pixels at a given pressure level, and dBZ_ind is the dBZ index. If there are no
251 hydrometeors in a pressure level, then the normalized mean dBZ index is set to 0. In
252 Figure 1 (c), the line with diamonds shows the vertical profile of the normalized mean
253 dBZ index for this cloud pattern.

254 There are two major benefits to expressing the vertical structure of a hydrometeor
255 pattern in this way. First, the vertical profile of the normalized mean dBZ index describes
256 the dominant hydrometeor system in a region. This is because higher radar reflectivity
257 roughly corresponds to larger particle sizes and cloud water contents. Rain and drizzle is
258 indicated by dBZ larger than ~ -15 (Frisch et al., 1995; Stephens and Woods, 2007)
259 whereas liquid clouds without rain or drizzle will have dBZ less than -15 and often less
260 than -30, in which case only the lidar can detect the cloud. For ice, thin cirrus clouds
261 typically have dBZ of -50 to -20 dBZ, whereas larger ice particles exhibit dBZ larger than

-20. Second, the use of a normalized mean dBZ index facilitates the comparison of observations with model simulations. This is because the model only predicts the grid-box mean cloud and precipitation condensate and thus assumptions would be necessary to reproduce the spread of dBZ often observed in clouds. Although we could use assumptions to generate the subgrid-scale variability in the simulator, the current version of the simulator distributes the model's cloud condensate and precipitation uniformly among the subgrid-scale columns designated to have cloud or precipitation, with the result that the histograms of signal strength are more narrow than is typically observed. A negative consequence of using the normalized mean dBZ index is that cloud coverage, a variable used in previous clustering analyses (Jakob 2003, Williams and Webb, 2008), is unused. This may not be a serious problem since the measurements, which are collected from a vertical curtain under the satellite track, may poorly estimate the cloud coverage in each 2-degree region. Note that while clustering is performed using the normalized mean dBZ index, all results in this paper are displayed using the joint histogram of atmospheric pressure and signal strength.

The clustering method iteratively searches for a predefined number of clusters starting with initial seeds. These seeds, used to create the initial cluster centroids, are selected randomly from the dataset with the only restriction being low correlation between any two seeds. The cluster centroids represent specific patterns in the vertical profile of the mean dBZ index. Every 2 degree CloudSat curtain is assigned to the cluster whose centroid has the minimum Euclidian distance in the vertical profile of the mean dBZ index. There are two ways to calculate the cluster centroids during the iterations. One is to recalculate the centroids after all elements are assigned to a cluster, and the other is to recalculate the cluster centroid each time an element is assigned to a cluster.

The latter way is used here because results depend less on the initial seeds chosen and the algorithm converges faster. To simply test the sensitivity of clustering results to initial seeds, the algorithm was repeated 30 times and a dominant set of cloud clusters is obtained in at least 75% of tests.

A limitation of the K-means algorithm is that the number of clusters needs to be subjectively specified in advance. Here the number of clusters is determined following the empirical criteria of Rossow et al. (2005). The correlation coefficients among the vertical profiles of the normalized mean dBZ index of the centroids and the geographical distributions of the frequency of occurrence of each cluster are used to judge the outcome. If the correlation between any two resulting clusters in both the centroid and the geographical distribution exceeds 0.7, the two clusters are designated as belonging to the same principal cloud regime. In the end step, subjective decisions are made to combine some of the resulting clusters and form a set of principal cloud regimes as has been done in previous studies (Williams and Tselioudis, 2007; Williams and Webb, 2008).

3. CFMIP observation simulator package (COSP)

To facilitate a meaningful comparison of the model with CloudSat and CALIPSO measurements, we use a simulator package which has been developed through international collaborations under the framework of the Cloud Feedback Model Intercomparison Project (CFMIP, http://cfmip.metoffice.com/CICCS.html). To avoid significant ambiguities in the direct comparison of model simulations with retrievals from observations, the CFMIP Observation Simulator Package (COSP) converts model clouds into pseudosatellite observations with a model to satellite approach that mimics the satellite view of an atmospheric column with model-specified physical properties. The approach accounts for observational limitations of the instruments.

COSP has three major parts: the generation of a subgrid-scale distribution of cloud and precipitation, the simulation of radar and lidar signals from this distribution, and the computation of statistical summaries from the subgrid-scale distribution of simulated signals which can then be compared to similar statistical summaries computed from observations. In the first part, each GCM grid box is equally divided into a number of vertical columns (50 in this case) and clouds are assigned to these columns in a manner consistent with the model's grid-box average stratiform and convective cloud amounts and its cloud overlap assumption. The scheme which produces a subgrid distribution of clouds is the Subgrid Cloud Overlap Profile Sampler (SCOPS) which is also used in the ISCCP simulator (Klein and Jakob, 1999; Webb et al. 2001). Note that the grid-box mean cloud condensate is divided equally among all columns that SCOPS designates as cloudy.

The next step is to determine which of the columns generated by SCOPS contain rain and snow. The scheme used is called SCOPS_PREC and is similar to that of Chevallier and Bauer (2003) and O'Dell et al. (2007). The inputs to SCOPS_PREC include the sub column distribution of large-scale and convective clouds from SCOPS and the model's grid-box mean precipitation flux of large-scale and convective rain and snow. Note that this scheme currently ignores any parameterization of precipitation area fraction that some models have (Jakob and Klein, 2000). To allow a close match between clouds allocated by SCOPS and precipitation produced by the clouds, precipitation is assigned to columns with the following algorithm which starts at the top-of-atmosphere and proceeds downward to the surface. There are in total five possibilities for the assignment of precipitation to columns, and they are used with different priorities. First, large-scale precipitation is assigned to all columns that either have stratiform clouds in the current level (possibility one) or large-scale precipitation in the level above

(possibility two). These two possibilities account for the overwhelming majority of cases. However, there may be rare instances where precipitation is not assigned after applying these possibilities. For these rare instances, the following possibilities are applied. The third possibility is to assign large-scale precipitation to all columns that have stratiform clouds in the level below. If precipitation is not assigned with the third possibility, then large-scale precipitation is assigned to all columns that have stratiform clouds anywhere in the vertical column (possibility four). If after this possibility, precipitation is still not assigned then it is assumed that large-scale precipitation covers 100% of the area and every column is filled with precipitation (possibility five). Possibility five is only used in the pathological case where the grid box has stratiform precipitation but no stratiform clouds. The same method is used to assign convective precipitation to columns using the convective clouds apportioned by SCOPS. The only difference is that convective precipitation is assumed to cover 5% of the area in possibility five. Following this assignment, the gridbox mean precipitation flux is, for lack of a better method, divided equally among all of the columns assigned to have precipitation. Then, the local precipitation flux is converted to a mixing ratio following Khairoutdinov and Randall (2003) who assume a Marshall-Palmer size distribution for precipitation and make a set of assumptions for particle terminal velocity.

In the second part of COSP, the radar and lidar signals are calculated using the column distribution of cloud and precipitation. The QuickBeam code (Haynes et al., 2007) is used to simulate the radar signal and calculates the vertical profiles of radar reflectivity accounting for attenuation of the radar beam from intervening hydrometeors, the atmospheric profiles of temperature and humidity, and assumptions for the particle size distributions of each hydrometeor. The ACTSIM code (Chiriaco et al. 2006; Chepfer

et al. 2007) is used to simulate the lidar signal and calculates the vertical profile of lidar backscatter from the same set of modeling variables excluding precipitation hydrometeors which contribute negligibly to the lidar backscatter. The simulated signals are considered valid where cloud optical depth is lower than about 2.5 and saturated if cloud optical depth exceeds this value. Aerosols are not currently included in the lidar simulator.

In the third part of COSP, statistical summaries are generated from these simulated signals in a manner similar to that used to derive the hydrometeor mask from the CloudSat and CALIPSO observations (Mace et al., 2008). In particular, we compute the joint histogram of atmospheric pressure and signal strength taking into account the radar sensitivity of -30 dBZ, surface contamination effects (Mace et al. 2007), and saturation of lidar signals. When the lidar detects cloud using a threshold value of normalized backscatter ratio of 3 and radar reflectivity is less than -30 dBZ, the occurrence frequency will contribute to the first column of the histogram. Volumes with radar reflectivity less than -30 dBZ that are beneath the level of complete attenuation of the lidar beam will be considered as clear. In these ways, the cloud and precipitation fields from model simulations are diagnosed in a manner as close as possible as the diagnosis with real observations.

While many sources of uncertainty can affact the output of COSP, two major uncertainties arise from the assumed particle size distributions for different hydrometeors and the methods used to generate subgrid-scale inhomogeneity in cloud condensate and precipitation. For example, Bodas-Salcedo et al. (2008) examined the role of the shape of the ice particle size distribution and found that the calculated radar reflectivity can change by around 5 dBZ from increasing or decreasing the intercept of the assumed

384 exponential distribution by a factor of 5. Since the signal bin width we select is 10 dBZ,
385 an uncertainty of this magnitude will not significantly change our conclusions. Further
386 exploration of uncertainties can be made by using the different distribution models
387 available in the radar simulator. The applicability of homogenous horizontal distribution
388 of cloud condensate and precipitation in subgrid scale and the cloud and precipitation
389 overlap are two important issues for an accurately simulated signal. Zhang et al. (2005)
390 found little sensitivity of model biases in comparison with ISCCP observations to the
391 replacement of randomly overlapped horizontally homogenous clouds with exponentially
392 decaying overlapped horizontally inhomogeneous clouds following the method reported
393 on in Pincus et al. (2006). For COSP, the signals will also be sensitive to the assumption
394 that the entire cloud generates precipitation and that the precipitation area does not
395 decrease beneath the cloud unless all of the precipitation evaporates. Testing the
396 sensitivity of the simulated signals to these assumptions will require future work. In the
397 context of this study, we will partially address the possible bias caused by distribution
398 assumptions by artificially homogenizing the observations to GCM gridbox scale (see
399 below).

400 Figure 2 displays a sample comparison between simulator output from CAM3.1
401 day-2 forecasts and the observations. It shows the east-to-west distribution of clouds in
402 the tropics formed as an average over tropical latitudes for June through September 2006.
403 CAM3.1 is able to capture some aspects of clouds related to the large-scale circulation
404 such as the abundance of clouds in the Asian Monsoon (70E through the dateline) and the
405 preferential occurrence of low clouds to the west of South America (80˚W to 160˚W) and
406 Africa (0˚W to 40˚W). However, it is clear that the model has too frequent high clouds
407 but too few mid- and low-level clouds. One interesting detail is that many CAM3.1

clouds have cloud water contents too small to be detected by either the radar or the lidar (This is the so-called "empty cloud" problem where cloud fraction is non-zero but cloud condensate is zero.). However, because these figures display averages over large temporal and spatial scales, they cannot indicate the exact disparities in cloud types between simulated and observed cloud systems. More detailed comparison is required to investigate whether the model can simulate specific clouds with the correct frequency in the right location. This motivates the following analysis of cloud regimes.

4. Clustering of tropical CloudSat and CALIPSO data

The results of applying the clustering method to CloudSat and CALIPSO observations are shown in Figures 3 and 4. These figures depict the cluster centroids in terms of the joint histogram of atmospheric pressure and signal strength (Figure 3) and the occurrence frequency maps of different cloud regimes (Figure 4). The different locations of maximum RFO for different cloud regimes is indicative of the association of cloud regimes with specific characteristics of the large-scale atmospheric circulation and thermodynamic states (Del Genio and Kovari, 2002; Rossow et al. 2005). Table 1 displays the tropical average relative frequency of occurrence and total cloud cover for each cloud regime.

Six cloud regimes are able to describe the variations of tropical cloud systems. Cloud regimes are given names based on the qualitative assessment of the joint histograms of atmospheric pressure and signal strength for each cluster (Figure 3). The first regime with an occurrence frequency of 35% (Table 1) is the most common cluster of the six, and is named as low cloud with less precipitation. Most of the clouds are detected by the lidar, and only a small fraction of clouds is detected by the radar. The second regime is named low cloud with precipitation due to the greater fraction of dBZ

values in excess of -15, which is an approximate threshold that distinguishes cloud from drizzle and rain (Frisch et al., 1995; Stephens and Wood, 2007). These two regimes are found with concentrations in the large subsidence regions of the tropical oceans (Klein and Hartmann, 1993). The first regime has the highest RFO at the west coasts of continents where marine stratocumulus clouds are known to be prevalent (Klein and Hartmann 1993). The second regime happens more frequently in regions where trade cumulus are predominant. Over warmer ocean temperatures than the first regime, the low clouds and precipitation extend deeper with clouds and precipitation occurring in the 680 to 800 hPa bin. The third regime is named thin cirrus and is characterized by clouds at high levels with low dBZ and sometimes only detectable by the lidar. This regime is most common in the Caribbean, the African Monsoon and the Asian Monsoon regions of India and South Asia. The fourth regime consists of clouds and precipitation over a wide range of dBZ below 440 hPa. This regime is suggestive of isolated convection that reaches the middle troposphere and will be named cumulus congestus. It often occurs as an important regime in the transition from shallow cumulus to deep convection. This regime is most common over the northwestern Pacific on the eastern edge of the Asian monsoon and with lesser frequency over the Inter-Tropical Convergence Zones of the Atlantic and Pacific oceans and the African and Asian monsoons. It also has a high RFO over the high topography of the west coast of South America, east central Africa, and South Asia. The fifth regime is named cirrus anvils and has a higher RFO at larger dBZ and occurs over a wider range of pressure as compared to the thin cirrus regime. This cloud type is generally produced by outflow from deep cumulus or synoptic and mesoscale disturbances (Sassen and Mace, 2002; Mace et al. 2006) and preferentially occurs over land areas in the monsoons of Asia, Africa, and Central America. The sixth and last

458 regime is named deep convection with heavy precipitation. It occurs most frequently in
459 the west Pacific warm pool and the Asian Monsoon region (Zipser et al., 2006; Liu and
460 Zipser, 2005).

461 By comparing these cloud regimes to those determined from an analysis of only
462 CloudSat data (Figure 1 in Zhang07), the value of combining the radar and lidar data is
463 readily apparent. First, the increase relative to Zhang07 of cloud RFO in the highest
464 pressure level for most regimes illustrates the capability of the lidar to sense tenuous
465 cirrus whose radar reflectivity is less than the radar detection threshold. Second, a large
466 portion of non-drizzling cumulus or stratocumulus are detected only by lidar as indicated
467 prominently by the two low-cloud regimes. Third, the lidar is capable of detecting thin
468 mid-level liquid water clouds particularly in the thin cirrus, congestus, and cirrus anvil
469 regimes. As a result, the occurrence of clear sky decreases from 30% in Zhang07 to 8%
470 in this study (Table 1). Note that clear sky is defined as when fewer than 5% of adjacent
471 200 profiles of satellite data have cloud or precipitation; obviously this number is
472 dependent on the number of profiles in the samples.

473
474 **5. Evaluation of CAM simulations**
475
476 ***5.1 CAM3.1***

477 Model data can be either clustered independently or assigned into the observational
478 cluster with the minimum Euclidian distance between the modeled and observed
479 normalized dBZ index. However, if model data are clustered independently, a different
480 number of clusters may result (Williams and Tselioudis, 2007). In this case, both the joint
481 histograms and the geographic distributions may differ substantially from the
482 observations leading to an ambiguous evaluation of model deficiencies. To reduce
483 complexity, model simulations are assigned to the cluster centroids determined from

484 observations, and the joint histograms formed by averaging the modeled elements in each
485 cluster are shown in Figure 5 with their corresponding RFO geographic distributions in
486 Figure 6. Tropical averages of the RFO and total cloud cover for each model regime are
487 reported in Table 1. Projecting model simulations onto the observed clusters allows one
488 to compare a common set of regimes.

489 Results indicate that the two model low level cloud regimes have much less than
490 observed hydrometeor fraction in their joint histograms of atmospheric pressure and
491 signal strength. In particular, the model has a strong underestimate of low level clouds
492 that are detectable only by the lidar. In contrast, the first low cloud regime has more
493 precipitating cloud than observed, and the intensity of drizzle for the two low cloud
494 regimes is too high compared with observations, reported recently elsewhere for other
495 models (Bodas-Salcedo et al., 2008; O'Connor et al., 2009). At the same time, the
496 modeled RFO of the first regime is much more frequent than observed in the oceanic
497 subsidence regions, while that of the second regime is much less frequent than observed
498 in these same regions. For both the thin cirrus and cirrus anvil regimes, the model has too
499 many clouds with dBZ larger than -10 albeit with a reasonable vertical profile of cloud
500 fraction in the upper troposphere. However, low clouds overlapped by high clouds are
501 underestimated in the model. The model simulates the thin cirrus regime nearly twice as
502 frequently as observed with strong overestimates over the Americas, the central Pacific
503 Ocean, and the Asian monsoon region. In the opposite direction, the model
504 underestimates the occurrence frequency of cumulus congestus by a factor of two with
505 prominent underestimates over the tropical west Pacific, the Asian monsoon region, east
506 central Africa, and the north part of South America. For this regime, the model
507 overestimates the occurrence of radar reflectivity above 10 dBZ suggesting that the

simulated mid-level clouds precipitate too heavily. For the deep convection with heavy precipitation regime, the hydrometeor coverage is lower than observed at levels beneath 440 hPa, while the frequency of this regime is strongly overestimated. The model radar reflectivity at middle levels is most frequent in the 10 to 20 dBZ range, while for observations the most frequent radar reflectivity occurs in the 0 to 10 dBZ range. Furthermore, the model frequency of large dBZ at lower levels is much less than observed, which may imply that an unrealistically large amount of model precipitation does not reach the surface. Regardless of the regime, a very prominent problem evident from the joint histograms is that the model strongly underestimates the occurrence of clouds with reflectivity less than -10, particularly clouds which are only detectable by the lidar. A separate comparison between the cloud optical thickness from model data and those derived from Moderate-Resolution Imaging Spectroradiometer (MODIS; Salomonson and Toll, 1991) measurements also illustrates the modeled clouds are too optically thick (not shown). These results indicate that the model clouds are too reflective, both at the frequency of the CloudSat radar but probably also at visible wavelengths (Zhang et al., 2005).

To investigate the effect of homogenous distribution of cloud condensate and precipitation, we create another set of the joint histograms for the observed cloud regimes by averaging up the measurements into grid-box (200 profiles) means and then calculate the joint histograms from the means using the cluster number determined by the original joint histograms without grid-box averaging (not shown). The comparison between this recalculated set and the simulations support that the model clouds are still too reflective for the two low clouds and two cirrus regimes, and that the model precipitation are too high. Note that this test probably overestimates the impact of the homogeneity

assumption, because the averaged histograms mix the cloud and precipitation together, while the model has a separate representation of cloud and precipitation.

In order to explore the relationship of model parameterizations to the discrepancies between models and observations, the simulator is run for convective and stratiform components of cloud systems separately and the resulting cloud patterns (not shown) are constructed using the assigned cloud regimes determined from the simulator output created from the complete cloud systems. For the low clouds with less precipitation regime, most model clouds are stratiform, while those for the low clouds with precipitation regime are both convective and stratiform but the mean convective dBZ is larger than the stratiform dBZ which unsurprisingly indicates stronger precipitation. For the thin cirrus and anvil cloud regimes, model clouds are predominantly stratiform, while the clouds of the cumulus congestus regime are from intense convective systems. The cloud coverage of the deep convection with heavy precipitation regime results equally from convective and stratiform systems. Unsurprisingly the dBZ of the convective clouds and precipitation are greater than that of the stratiform clouds and precipitation, and the modeled stratiform precipitation is less frequent beneath 680 hPa than above which is suggestive of precipitation evaporation in the lower troposphere. Considering that the model dBZ is too great, that the area of precipitation is too low, and that the RFO is too great for this regime, it appears that the model produces too much convective precipitation but too little stratiform precipitation. This result is consistent with that of Dai (2006) who found that this model (as well as most atmospheric models) underestimate/overestimate the accumulated stratiform/convective precipitation in the tropics based on TRMM observations.

5.2 CAM3.5

556 Applying the same analysis approach to cloud simulations from CAM3.5 yields
557 joint histograms for the six regimes (Figure 7) that are nearly identical to those from
558 CAM3.1. However, the differences in the RFO and spatial distributions are remarkable
559 (Figure 8 and Table 1). First, the occurrence frequency and total cloud coverage of thin
560 cirrus decreases dramatically with similar but smaller changes for the cirrus anvil and
561 deep convection regimes. In particular, the decrease in the occurrence frequency of thin
562 cirrus from 16% to 10% corrects a strong overestimate of the observed occurrence
563 frequency of 9%. Second, the occurrence frequency of low clouds with precipitation
564 increases from 14% to 22% with the regime occurring in more extensive oceanic regions
565 in better agreement with observations. This increase generally comes at the expense of
566 the low clouds with less precipitation regime whose occurrence is now limited more to
567 the marine stratocumulus regions also in better agreement with observations. Finally, one
568 of the most impressive improvements is that CAM3.5 has a strong increase in the
569 occurrence frequency of congestus from 5% to 10% which is now in agreement with the
570 observed occurrence frequency of 9%.

571 It is tempting to attribute most of the improvements in the regime occurrence
572 frequencies to the elimination of undilute plumes in the deep convection parameterization
573 of CAM3.5. Indeed, this is confirmed by examination of a separate integration of
574 CAM3.5 modified to permit undilute plumes according to the formulation that was used
575 in CAM3.1 (Table 1). Physically, dilute plumes have detrainment levels in the middle
576 and lower troposphere and the inclusion of the dilute plumes likely explains the increase
577 in the occurrence frequency of low clouds with precipitation and congestus, and the
578 decrease in the occurrence frequency of deep convection. Indeed, in the simulation of
579 CAM3.5 with undilute plumes, the occurrence frequency of low clouds with precipitation

580 decreases from 22% to 16% and the occurrence frequency of congestus decreases from
581 10% to 5%, confirming that the change in the dilution of convective plumes is
582 responsible for most of the increase of these regimes from CAM3.1 to CAM3.5. The
583 reduction in the occurrence frequency and total cloud coverage of thin cirrus that results
584 from dilute plumes (Table 1) may be the result of decreased condensate and water vapor
585 detrainment from deep convection in the upper troposphere. This interpretation is
586 consistent with the strong decrease in the occurrence frequency of the deep convection
587 with heavy precipitation regime in CAM3.5 (Table 1).

588 ***5.3 The association of cloud regimes with large-scale dynamics***

589 To explore the coupling between cloud regimes and the large-scale dynamics that is
590 supportive of different cloud types, the occurrence frequency of cloud regimes from both
591 observations and model simulations over ocean are sorted by the value of monthly mean
592 vertical pressure velocity at 500 hPa (ω_{500}). Although cloud systems may be associated
593 with other large-scale parameters, such as sea surface temperature or lower tropospheric
594 stability (Klein and Hartmann, 1993; Weaver, 1999; Williams et al., 2003; Ringer and
595 Allan, 2004), we choose to examine ω_{500} because of its recent widespread use in the
596 analysis of tropical clouds following the pioneering approach of Bony et al. (2004).
597 NCEP vertical velocities are sorted into 8 bins such that the occurrence frequency of each
598 bin is equal. The compositing of observed cloud regimes into vertical velocity bins is
599 performed in two ways (Figure 9). In the first way, the fraction of elements of a given
600 regime which occur in a given vertical velocity bin is displayed in Figure 9a. If there
601 were no relationship between a cloud regime and ω_{500}, the occurrence frequency of a
602 regime in each velocity bin would be equal to 0.125 apart from random fluctuations. In
603 the second way, the fraction of elements in a given vertical velocity bin which belong to a

given regime is displayed in Figure 9b. In this way, the sum of the frequencies for the six regimes in each velocity bin is 1. As expected, the two low cloud regimes are much more common in subsidence regions and the remaining regimes are more common in ascent regions. The association of cloud regimes with large-scale dynamics provides quantitative targets for model simulations.

Figure 10 displays differences between observations and CAM3.1 and CAM3.5 simulations. Compared with observations (Figure 10a) CAM3.1 overestimates the occurrence frequency of deep convection with heavy precipitation in the three dynamic regimes with the strongest upward motion. In contrast, congestus are underestimated but thin cirrus are overestimated not only in the strongly ascending regimes, but also in the relatively weakly ascending and descending regimes. In descending regimes, the model produces too many low clouds with less precipitation but too few low clouds with precipitation. However, in strongly ascending regimes the model underestimates both of these low cloud regimes.

The impact of the model changes between CAM3.1 and CAM3.5 on the frequency of cloud regimes in different dynamical regimes is displayed in Figure 10b. The occurrence frequency of congestus in each dynamic regime rises with stronger increases in the ascending regimes. Likewise the occurrence frequency of thin cirrus decreases in all regimes, but with larger decreases in ascending regimes. The occurrence frequency of deep convection with heavy precipitation has moderate decreases in the second and third bins with upward motion although this does not cancel completely the model overestimate. In nearly all regimes, the occurrence frequency of low clouds with precipitation increases, but the decreases in the occurrence frequency of low cloud with less precipitation are limited to descending regimes. As a result, cloud simulations from

628 CAM 3.5 compare more closely to the observations than those of CAM 3.1 as shown in
629 Figure 10c. In terms of occurrence frequency, the primary error is that deep convection
630 still happens too frequently in ascending regimes while low cloud with less precipitation
631 happen too infrequently in these same regimes. This suggests that the deep convection
632 parameterization is still acting too frequently in CAM3.5 perhaps at times when only low
633 clouds should occur.

634 ***5.4 Comparison between CAM3's forecasts and its climate***

635 In order to examine the consistency between cloud regimes of CAM3's climate and
636 its forecasts, data from 'climate' integrations of CAM3 using only observed sea-surface
637 temperatures and sea ice for June-September 2006 are analyzed following the method
638 used for the forecasts. The joint histograms of atmospheric pressure and signal strength of
639 the six regimes from the climate integrations are similar to those of the forecasts, but the
640 RFO of the individual cloud regimes have several noticeable differences. In the climate
641 integrations of both CAM3.1 and CAM3.5, the low clouds with precipitation regime is
642 more common in the subsidence regions, and the congestus regime occurs more
643 frequently in ascending regimes. In contrast, the deep convection with heavy
644 precipitation regime is less frequent in the climate integrations than that from the
645 forecasts.

646 To show the relationship between cloud regimes and the 500 hPa pressure vertical
647 wind, frequency differences similar to Figure 10 are created for the climate integrations
648 (Figure 11). Although the differences with observations are not the same, the differences
649 between CAM3.1 and CAM3.5 for almost all cloud regimes in climate integrations are
650 similar to those of the forecasts. For example, low clouds with precipitation increase at
651 the expense of low clouds with less precipitation, and the congestus clouds occur more

652 frequently in ascending regions. However, it is not obvious which version of the model
653 generates cloud simulations more close to observations. For the simulations of CAM 3.5,
654 although deep convection with heavy precipitation is reduced in the regions with strong
655 upward motion, the occurrence of the congestus clouds is too frequent and that of low
656 clouds with less precipitation is too infrequent compared with the observations.
657
658 **6. Summary**
659
660 This paper uses tropical measurements of cloud fields from CloudSat and CALIPSO
661 to evaluate cloud simulations from the CAM3. The merged CloudSat and CALIPSO
662 dataset provides the most accurate description of the vertical structure of hydrometeor
663 fields currently possible on a global basis. It has the potential to advance our
664 understanding of cloud processes and improve model evaluations. Observations are
665 analyzed in terms of cloud regimes using a clustering technique applied to tropical data
666 for the period June to September 2006. Six cloud regimes with distinctive cloud
667 mesoscale patterns to the vertical profiles of signal strength are identified, and the
668 geographical distributions of the occurrence frequencies of these principal cloud regimes
669 illustrate the association with the large-scale atmospheric circulation.
670 A satellite simulator package is applied to the model to aid quantitative evaluation of
671 model performance using the new data. The joint histograms of atmospheric pressure and
672 signal strength generated by the simulator package are used to assess model performance
673 under the clustering framework. Assigning model histograms to the observed cloud
674 regimes facilitates comparison in terms of both the occurrence frequency and properties
675 of cloud regimes.
676 The comparison of the geographical distributions between model simulations and
677 observations shows that CAM3.1 overestimates the occurrence of high clouds especially

678 in the Tropical Western Pacific, east central Africa, and northern South America, and
679 underestimates the occurrence of low clouds with precipitation and congestus. Although
680 similar differences have been found in many previous studies (Zhang et al. 2005;
681 Williams and Tselioudis 2007), generally they used traditional satellite observations
682 which are based on vertically integrated measurements. Due to the limitations of passive
683 remote sensing in determining the location of cloud layers, it is necessary to establish the
684 robustness of model evaluations by considering observations from active remote sensors
685 that accurately determine the vertical structure of clouds and precipitation.

686 Differences in the joint histograms of atmospheric pressure and signal strength are
687 able to expose model deficiencies in the simulated hydrometeor properties. It is found
688 that cloud coverage of the two low cloud regimes and congestus regimes are significantly
689 lower than observed. Low- and mid-level clouds may precipitate too heavily. The biases
690 in the joint histogram for the deep convection with heavy precipitation regime suggests
691 that the model overestimates convective precipitation but underestimates stratiform
692 precipitation, and not enough precipitation from stratiform clouds reaches the surface. In
693 general, the modeled clouds are too reflective in all regimes, which is consistent with that
694 seen by Bodas-Salcedo et al. (2008) who used CloudSat data to evaluate clouds and
695 precipitation in the Unified Model of the United Kingdom Meteorological Office. Also, it
696 is particularly prominent in the fact that the model is unable to simulate hardly any clouds
697 with radar reflectivity less than -30 but still detectable by CALIPSO, and a similar result
698 was found with the French climate model (Chepfer et al. 2008).

699 To examine the impact of model parameterizations on the simulated clouds, we also
700 evaluate CAM 3.5. The cloud mesoscale patterns of CAM3.5 are similar to those from
701 CAM 3.1, but the geographical distributions of the RFO are significantly different. The

new version of the model reduces deep convection and high clouds and produces more congestus and low clouds with precipitation. These changes are primarily due to implementation of dilute plumes in the deep convection parameterization which leads to greater detrainment in the middle troposphere and less detrainment in the upper troposphere.

The cloud regimes are also sorted by the monthly mean vertical wind at 500 hPa to show the relationship between tropical cloud systems and the large-scale environment that influences the evolution of cloud systems. It is shown that, relative to CAM3.1, CAM3.5 suppresses deep convection with heavy precipitation and generates more congestus in ascending regions and low clouds with precipitation in subsidence regions. However, deep convection is still too frequent in strongly ascending regions, while low clouds are still too infrequent.

Although results from climate integrations of CAM show different geographical distributions of the occurrence frequencies for the individual cloud regimes relative to those of the forecasts, the changes from CAM3.1 to CAM3.5 are identical for all the regimes. The differences of cloud simulations between forecasts and climate integrations may imply that the feedback processes are partly responsible for the climatological biases. Our result is not consistent with that in Williams and Brooks (2007), which found the cloud regimes are similar for the forecasts and the climate integrations with the Met Office Unified Forecast-Climate Model. The lack of differences in cloud regimes between forecasts and climate integrations may be partly due to the fact that the analysis used to initialize their climate model is from a data-assimilation system with the same physical model. Further investigation of the spin-up of model clouds and precipitation in CAM3 is warranted.

Although some of the conclusions from this study echo those of previous cluster studies using passive satellite (ISCCP) data, some new perspectives are provided. In particular, the fact that the CPR can see precipitation allows one to diagnose errors in model precipitation simulations together with cloud errors. One surprising result is that the CAM3.5 has as much or greater amounts of congestus as observations. This contrasts with all previous studies using ISCCP data which had concluded that models lack congestus clouds. A possible reconciliation between these results comes from the fact that we primarily use precipitation profiles in this study to detect congestus whereas the other studies using ISCCP data rely on identification of congestus through the visible and infrared cloud properties. If the results from the CAM are typical, it may be that models do produce congestus (middle level topped precipitating convection) but that the cloud properties of the congestus regime are seriously biased. Indeed, a preliminary comparison of ISCCP simulator results when the CAM simulates congestus clouds (as identified by CloudSat) suggests that the model cloud properties for the congestus regime are indeed biased when compared to MODIS observations of visible optical thickness and highest cloud top pressure.

In the future, we will exploit the synergy of the A-Train to deliver complementary measurements of the same environmental phenomena and the collocated large-scale variables along the CloudSat flight track, to further understand model deficiencies. For example, Clouds and the Earth's Radiant Energy System (CERES; Wielicki et al., 1996) radiative fluxes will be used to describe the radiative characteristics of the individual regimes and address the impact of the cloud regimes on the cloud radiative forcing at the top of atmosphere.

Acknowledgements:

This work was funded through a grant from the NASA Modeling and Analysis and Prediction Program, Don Anderson, program manager. This research was performed under the auspices of the U.S. Department of Energy by Lawrence Livermore National Laboratory under contract DE-AC52-07NA27344. Support for this work (GM) at the University of Utah was provided by NASA through a contract issued by the Jet Propulsion Laboratory, California Institute of Technology under a contract with NASA. We greatly appreciate the information from DIME website for the cluster program. We also thank Richard Neale for assistance in constructing the simulation of CAM3.5 with undilute plumes.

Reference:

Anderberg, M. R. (1973), Cluster Analysis for Applications, 359 pp., Academic, New York.

Bodas-Salcedo A., M. J. Webb, M. E. Brooks, M. A. Ringer, K. D. William, S. F. Milton, D. R. Wilson, 2008: Evaluating cloud systems in the Met Office global forecast model using simulated CloudSat radar reflectivities. J. Geophys. Res., 113, D00A13, doi:10.1029/2007JD009620.

Bony, S., et al. (2004), On dynamic and thermodynamic components of cloud changes, Clim. Dyn., 22, 71– 86.

Bony, S., R. Colman, V. M., Kattsov, R. P. Allan, C. S. Bretherton, J-L. Dufresne, A. Hall, S. Hallegatte,M. M. Holland, W. Ingram, D. A. Randall, B. J. Soden, G. Tselioudis, and M. J. Webb, 2006: How well do we understand and evaluate climate change feedback processes? J. Climate, 19, 3445-2461.

Boccippio, D. J., W. A. Petersen, and D. J. Cecil, 2005: The tropical convective spectrum. Part I: Archetypal vertical structures. *J. Clim.*, **18**, 2744-2769.

Cess, R. D., and co-authors, 1990: Intercomparison and interpretation of climate feedback processes in 19 atmospheric general circulation models. J. Geophys. Res., 95, D10, 16,601-16,615.

Chen, Y., and A. D. Del Genio, 2008: Evaluation of tropical cloud regimes in observations and a general circulation model. Clim. Dyn., 32, 355-369.

Chevallier, F., and P. Bauer, 2003: Model rain and clouds over oceans: Comparison with SSM/I observations. Mon. Wea. Rev., 131, 1240-1255.

Chiriaco, M., et al., 2006: The ability of MM5 to simulate ice clouds: systematic comparison between simulated and measured fluxes and Lidar/Radar profiles at the SIRTA atmospheric observatory. Mon Weather Rev, 134, 897-918.

Chepfer, H., M. Chiriaco, R. Vautard, and J. Spinhirne, 2007: Evaluation of MM5 Optically Thin Clouds over Europe in Fall Using ICESat Lidar Spaceborne Observations. Mon Weather Rev, 135, 2737-2753.

Chepfer, H., S. Bony, D. Winker, M. Chiriaco, J.-L. Dufresne, G. Sèze, 2008: Use of CALIPSO lidar observations to evaluate the cloudiness simulated by a climate model. Geophys. Res. Lett., 35, L15704, doi:10.1029/2008GL034207.

Collins, W. D., et al., 2006: The formulation and atmospheric simulation of the Community Atmospheric Model: CAM3. J. Clim., 19, 2144-2161.

Dai, Aiguo, 2006: Precipitation characteristics in eighteen coupled climate models. J. Clim., 19, 4605-4630.

811 Del Genio, A. D., and W. Kovari, 2002: Climatic properties of Tropical precipitating
812 convection under varying environmental conditions. J. Climate, 15, 2597-2615.
813
814 Frisch, A. S., C. W. Fairall, and J. B. Snider, 1995: Measurement of stratus cloud and
815 drizzle parameters in ASTEX with Ka-band Doppler radar and microwave radiometer.
816 J. Atmos. Sci., 52, 2788-2799.
817
818 Haynes, J. M., G. L. Stephens, 2007: Tropical oceanic cloudiness and the incidence of
819 precipitation: Early results from Cloudsat. Geophys. Res. Lett., L09811 DOI
820 10.1029/2007GL029335.
821
822 Houghton, J.T., and et al., 2001: Climate change: the scientific basis. Contribution of
823 working group I to the third assessment report of the intergovernmental panel on
824 climate change. Cambridge University Press, Cambridge, pp 525-582.
825
826 Im, E., S. L. Durden, and C. Wu, 2006: Cloud Profiling Radar for the CloudSat mission.
827 IEEE Aerosp. Electron. Syst. Mag., 20, pp. 15-18.
828
829 Jakob, C., and G. Tselioudis (2003), Objective identification of cloud regimes in the
830 Tropical Western Pacific, Geophys. Res. Lett., 30(21), 2082, doi:
831 10.1029/2003GL018367.
832
833 Jensen, M. P., and A. D. Del Genio, 2006: Factors limiting convective Cloud-Top height
834 at the ARM Nauru Island climate research facility. J. Climate, 19, 2105-2117.
835
836 Klein, S. A., and D. L. Hartmann, 1993: The seasonal cycle of low stratiform clouds. J.
837 Climate, 6, 1587-1606.
838
839 Klein, S. A., X. Jiang, J. Boyle, S. Malyshev, S. Xie, 2006: Diagnosis of the summertime
840 warm and dry bias over the U.S. Southern Great Plains in the GFDL climate model
841 using a weather forecasting approach, Geophys. Res. Lett., 33, L18805,
842 doi:10.1029/2006GL027567.
843
844 Klein, S. A, and C. Jakob, 1999: Validation and sensitivities of frontal clouds simulated
845 by the ECMWF model. Mon Weather Rev, 127(10):2514-2531.
846
847 Khairoutdinov, M. F., and D. A. Randall, 2003: Cloud resolving modeling of the ARM
848 Summer 1997 IOP: Model formulation, results, uncertainties, and sensitivities, J.
849 Atmos. Sci., 60, 607-625.
850
851 Liu, C. and E. J. Zipser, 2005: Global distribution of convection penetrating the tropical
852 tropopause. *J. Geophys. Res.*, **110**, D23104.
853
854 Liu, C. and E. J. Zipser, 2008: Diurnal cycles of precipitation, clouds, and lightning in the
855 tropics from 9 years of TRMM observations. Geophys. Res. Lett., 35, L04819,
856 doi:10.1029/2007GL032437.
857
858 Mace, G. G. (2004), Level 2 GEOPROF product process description and interface control

document, Coop. Inst. for Res. in the Atmos., Fort Collins, Colo.

Mace, G.G., M. Deng, B. Soden, E. Zipser, 2006: Association of tropical cirrus in the 10-15-km layer with deep convective sources: an observational study combining Millimeter Radar data and satellite-derived trajectories. J. Atmos. Sci., 63, 480-503.

Mace, G. G., R. Marchand, Q. Zhang, and G. Stephens (2007), Global hydrometeor occurrence as observed by CloudSat: Initial observations from summer 2006, Geophys. Res. Lett., 34, L09808, doi:10.1029/2006GL029017.

Mace, G. G., and et al., 2008: A Description of Hydrometeor Layer Occurrence Statistics Derived from the First 4 Year of Merged Cloudsat and CALIPSO Data. J. Geophys. Res., Accepted.

Marchand, R. T. Mace. G.G., and Ackerman T.P. 2008: "Hydrometeor Detection using CloudSat - an Earth Orbiting 94 GHz Cloud Radar", J. of Atmos. Oceanic Technol., 25, 519-533, doi:10.1175/2007JTECHA1006.1.

Neale, R. B., J. H. Richter, and M. Jochum (2008), The impact of convection on enso: From a delayed oscillator to a series of events, Journal of Climate, preprint (2008), 0000–0000

Norris, J. R., and C. P. Weaver (2001), Improved techniques for evaluating GCM cloudiness applied to the NCAR CCM3, J. Clim., 14, 2540–2550.

O'Connor, E. J., R. J. Hogan, A. J. Illingworth, and C. D. Westbrook, 2009: How do model parameterizations of drizzle compare to radar and lidar observations? J. Climate., submitted.

O'Dell, C. W., P. Bauer, R. Bennartz, 2007: A Fast Cloud Overlap Parameterization for Microwave Radiance Assimilation. J. Atmos. Sci., 64, 3896-3909.

Phillips, T. J., et al., 2004: Evaluating parameterizations in GCMs: Climate simulation meets weather prediction. Bull. Am. Meteorol. Soc., 85,1903-1915.

Pincus, Robert, R. Hemler, and S. Klein, 2006: Using stochastically generated subcolumns to represent cloud structure in a Large-scale model. Monthly Weather Rev., 134, 3644-3656.

Randall, D. A., and et al., 2007: Climate models and their evaluation. In Climate Chanfe 2007: The Physical Science Basis. Contribution of Working Group I to the Fourth Assessment Report of the Intergovernmental Panel on Climate Change [Solomon, S., D. Qin, M. Manning, Z. Chen, M. Marquis, K.B. Averyt, M. Tignor and H. L. Miller(eds.)]. Cambridge University Press, Cambridge, United Kingdom and New York, NY, USA.

Ringer, M., and R. Allan, 2004: Evaluating climate model simulations of tropical cloud. Tellus A 56:308-327.

907
908 Richter, J. H., and P. J. Rasch (2008), Effects of convective momentum transport on the
909 atmospheric circulation in the community atmopshere model, version 3 (cam3), J.
910 Climate.
911
912 Rossow, W. B., G. Tselioudis, A. Polak, and C. Jakob (2005), Tropical climate described
913 as a distribution of weather states indicated by distinct mesoscale cloud property
914 mixtures, Geophys. Res. Lett., 32, L21812, doi:10.1029/2005GL024584.
915
916 Rossow, W. B., and R. A. Schiffer: Advances in understanding clouds from ISCCP. *Bull. Amer. Meteor. Soc.,* 80, 2261-2288, 1999.
917
918
919 Salomonson, V. V., and D. L. Toll, 1991: Execution phase (C/D) spectral band
920 characteristics of the EOS Moderate Resolution Imaging Spectrometer-Nadir
921 (MODIS-N) facility instrument. Adv. Space Res., 11, 231-236.
922
923 Sassen, K., and G. G. Mace, 2002: Cirrus. Ground-Based Remote Sensing of Cirrus
924 Clouds. D. K. Lynch et al., Eds., Oxford University Press, 168-196.
925
926 Stephens, G. L., et al. (2002), The CloudSat mission and the A-Train, Bull. Am. Meteorol.
927 Soc., 83, 1771–1790.
928
929 Stephens, G. L., and N. B. Wood, 2007: Properties of tropical convection observed by
930 Millimeter-Wave Radar Systems. Mon. Wea. Rev., 135, 821-842.
931
932 Soden, B. J., A. J. Broccoli, R. S. Hemler, 2004: On the use of cloud forcing to estimate
933 cloud feedback. J. Climate, 17(19): 3661-3665.
934
935 Soden, B. J., and I. M. Held, 2006: An assessment of climate feedbacks in coupled ocean
936 atmosphere models. J. Climate, 19, 3354-3360.
937
938 Wielicki, B. A., B. R. Barkstrom, E. F. Harrison, R. B. Lee III, G. L. Smith, and J. E.
939 Cooper, 1996: Clouds and the Earth's Radiant Energy System (CERES): An Earh
940 observing system experiment. Bull. Am. Meteorol. Soc., 77, 853-868.
941
942 Webb, M., C. Senior, S. Bony, J. J. Morcrette, 2001: Combining ERBE and ISCCP data
943 to assess clouds in the Hadley Centre, ECMWF and LMD atmospheric climate
944 models. Clim Dyn, 17:905-922.
945
946 Williams, K. D., C. A. Senior, J. Mitchell, 2001: Transient climate change in the Hadley
947 Centre models: the role of physical processes. J. Climate, 14, 12:2659-2674.
948
949 Williams, K. D., M. A. Ringer, C. A. Senior, 2003: Evaluating the cloud response to
950 climate change and current climate variability. Clim. Dyn, 20, 705-721.
951
952 Williams, K. D., C.A. Senior, A. Slingo and J.F.B. Mitchell, 2005: Towards evaluating
953 cloud response to climate change using clustering technique identification of cloud
954 regimes. Clim. Dyn. 24, 701-719 doi:10.1007/s00382-004-0512-z.

Williams, K. D., and et al., 2006: Evaluation of a component of the cloud response to climate change in an intercomparison of climate models. Clim. Dyn., 26, 145-165. Doi 10.1007/s00382-005-0067-7.

Williams, K. D., and G. Tselioudis, 2007: GCM intercomparison of global cloud regimes: present-day evaluation and climate change response. Climate Dynamics, 29, 231-240.

Williams, K. D., and M. Webb, 2008**:** A quantitative performance assessment of cloud regimes in climate models Clim. Dyn. In press.

Winker, D. M., B. H. Hunt, and M. J. McGill (2007), "Initial performance assessment of CALIOP", Geophys. Res. Lett., 34, L19803, doi:10.1029/2007GL030135

Xie, S. C., J. Boyle, S. Klein, X. Liu, and S. Ghan, 2008: Simulations of Arctic mixed-phase clouds in forecasts with CAM3 and AM2 for M-PACE. J. Geophys. Res., 113, D04211, doi: 10.1029/2007JD009225.

Zipser, E. J., et al. (2006), Where are the most intense thunderstorms on Earth?, Bull. Am. Meteorol. Soc., 87, 1057–1071.

Zhang, G. J., and N. A. McFarlane 1995:Sensitivity of climate simulations to the parameterization of cumulus convection in the Canadian Climate Center general circulation model, Atmos. Ocean, 33, 407-446.

Zhang, M., W. Lin, C. S. Bretherton, J. J. Hack, and P. J. Rasch, 2003: A modified formulation of fractional stratuform condensation rate in the NCAR Community Atmospheric Model (CAM2). J. Geophys. Res., 108, 4035, doi:10.1029/2002JD002523.

Zhang, M. H., and co-authors, (2005), Comparing Clouds And Their Seasonal Variations in 10 Atmospheric General Circulation Models With Satellite Measurements, *J. Geophys. Res., 110,* D15s03, doi:10.1029/2004JD005021.

Zhang, Y., and G. G. Mace, 2006: Retrieval of Cirrus Microphysical Properties with a Suite of Algorithms for Airborne and Spaceborne Lidar, Radar, and Radiometer Data. J. Appli. Meteorol. And Climatol., 45, 1665-1689.

Zhang Y., S. Klein, G. G. Mace, J. Boyle (2007), Cluster analysis of tropical clouds using CloudSat data, Geophys. Res. Lett., 34, L12813, doi:10.1029/2007GL029336.

Zhang, Y., S. A. Klein, C. Liu, B. Tian, R. T. Marchand, J. M. Haynes, R. B. McCoy, Y. Zhang, and T. P. Ackerman, 2008: On the diurnal cycle of deep convection, high-level cloud, and upper troposphere water vapor in the Multiscale Modeling Framework, J. Geophys. Res., 113, D16105, doi:10.1029/2008JD009905.

	low clouds with less precip		low clouds with precip		thin cirrus		congestus		cirrus anvils		deep convection with heavy precip		Clear
	RFO	TCC	RFO	TCC	RFO	TCC	RFO	TCC	RFO	TCC	RFO	TCC	RFO
Observation	35%	0.63	18%	0.69	9%	0.84	9%	0.84	8%	0.90	13%	0.93	8%
CAM 3.1	31%	0.36	14%	0.35	16%	0.70	5%	0.45	7%	0.88	24%	0.84	3%
CAM 3.5 undilute	29%	0.31	16%	0.32	14%	0.62	5%	0.41	6%	0.82	26%	0.84	4%
CAM 3.5	26%	0.27	22%	0.26	10%	0.50	10%	0.35	7%	0.73	21%	0.78	4%

Table 1. The data distributions for observations, simulations from CAM3.1, CAM3.5 with undilute plume, and CAM3.5 in the six cloud clusters and clear-sky condition with TCC lower than 5%. The data listed are the relative frequency of occurrence (RFO, left column), and the total cloud coverage (TCC, right column). The numbers of elements are 54,828 and 913,536 for observations and model simulations, respectively.

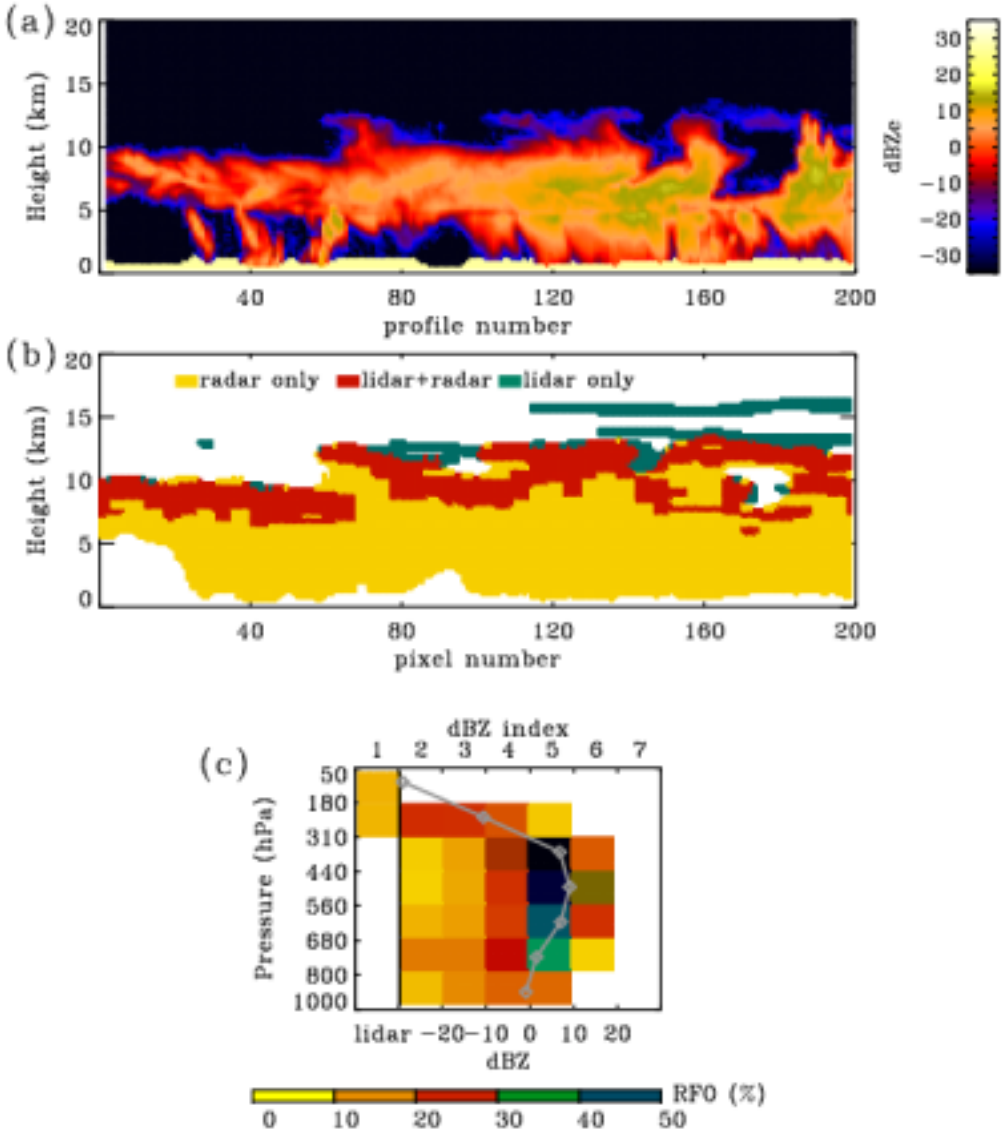

Figure 1. A case from Tropical Western Pacific Ocean (2°N 140°E) on Jul 15, 2006 that illustrates the creation of the joint histogram of atmospheric pressure and signal strength for a mesoscale cloud pattern. (a) radar reflectivity from CloudSat observations of 200 adjacent profiles (b) hydrometeor mask by combining radar and lidar data (c) the joint histogram of atmospheric pressure and signal strength for this sample. The shading indicates the relative frequency of occurrence (RFO) of clouds or precipitation at each bin of atmospheric pressure; The left column depicts the cloud fraction detected by lidar but missed by radar ('lidar only' clouds in panel b); The line with diamonds depicts the vertical profile of the normalized mean dBZ index for this histogram.

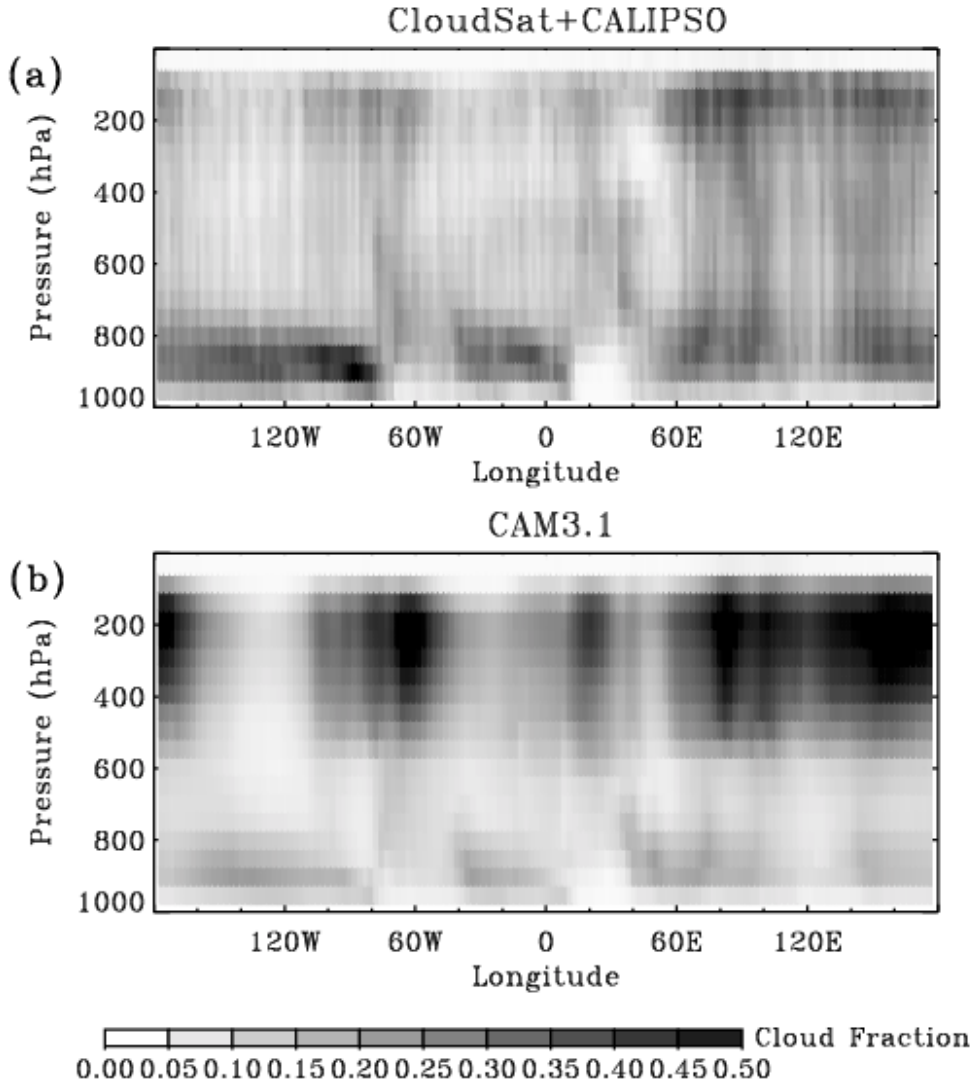

Figure 2. Comparison of the meridional-mean cloud occurrence frequency for the tropical region (23.5˚S-23.5˚N) during June-September 2006: (a) Observations from CloudSat and CALIPSO (b) Simulator output of the cloud simulations from CAM 3.1 day-2 forecasts.

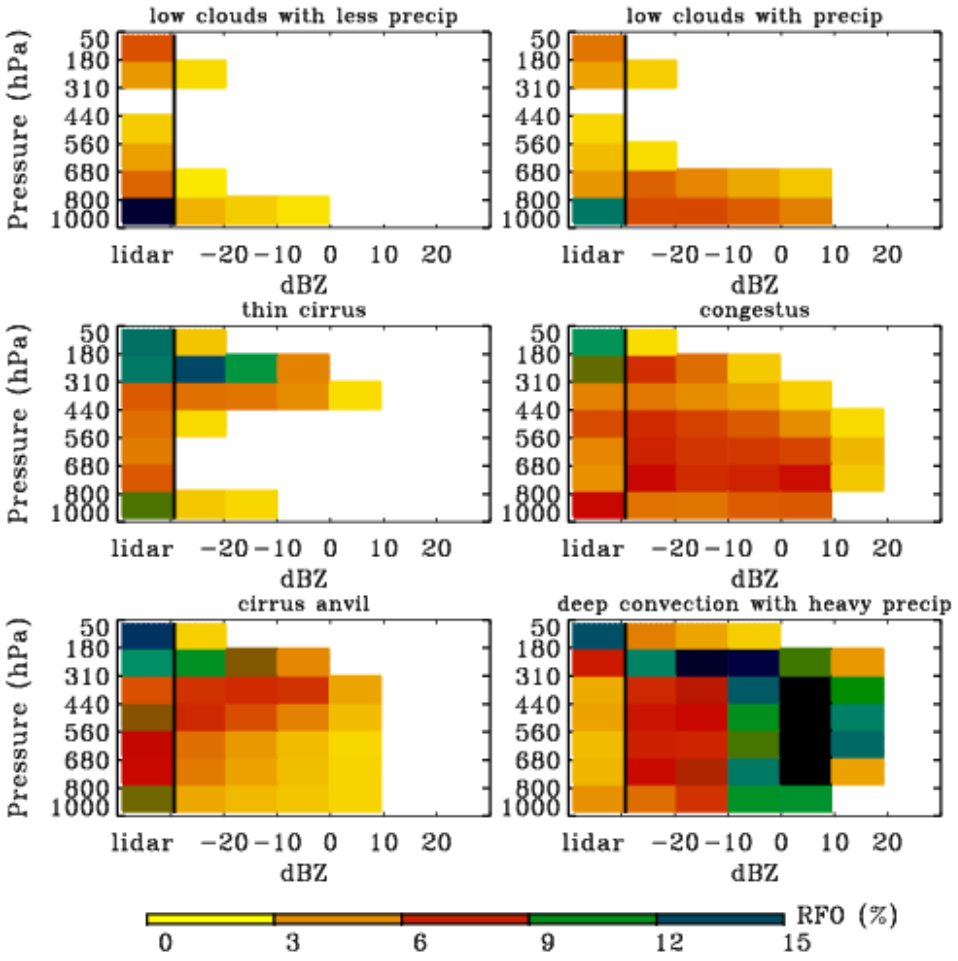

Figure 3. Joint histograms of atmospheric pressure and signal strength for the centroids of the six tropical clusters from the CloudSat and CALIPSO observations collected in June-September 2006. These clusters are named by the primary cloud morphology.

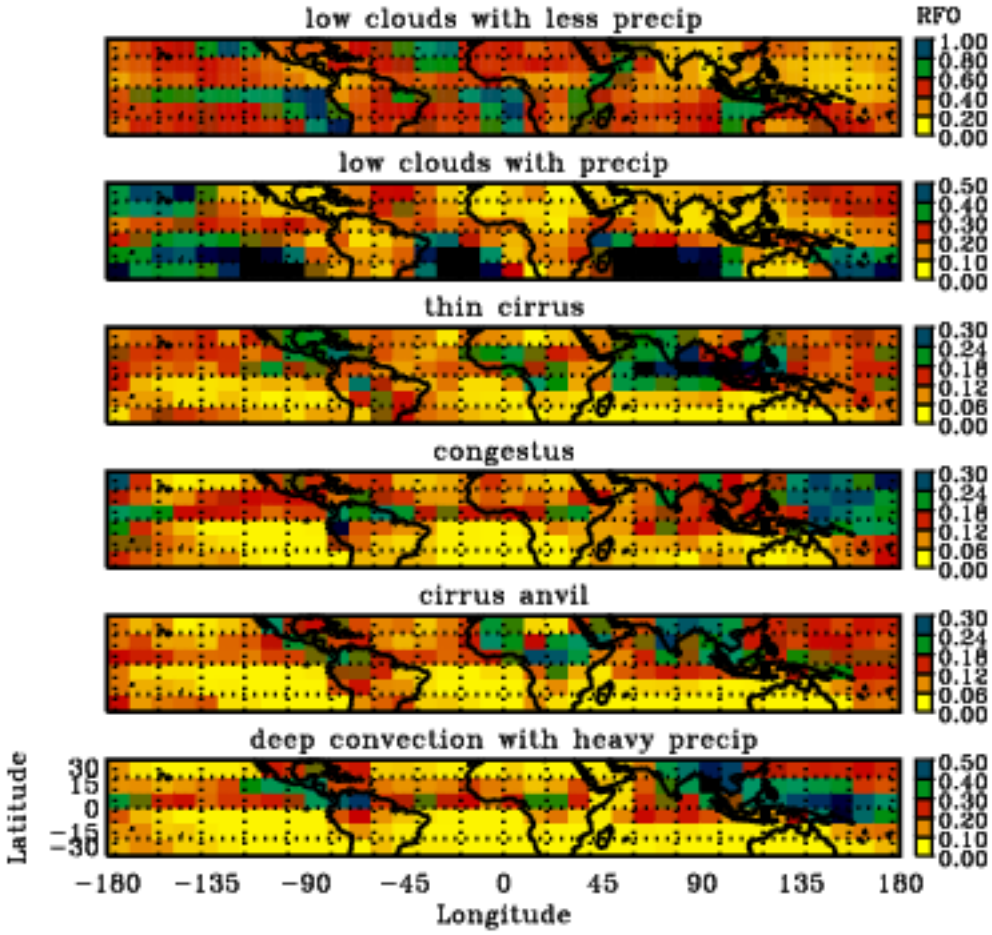

Figure 4. The time-averaged occurrence fraction of each CloudSat-CALIPSO cluster. The sum of the frequencies across clusters represents the frequency of cloudy patterns in a 10˚-by-10˚ box.

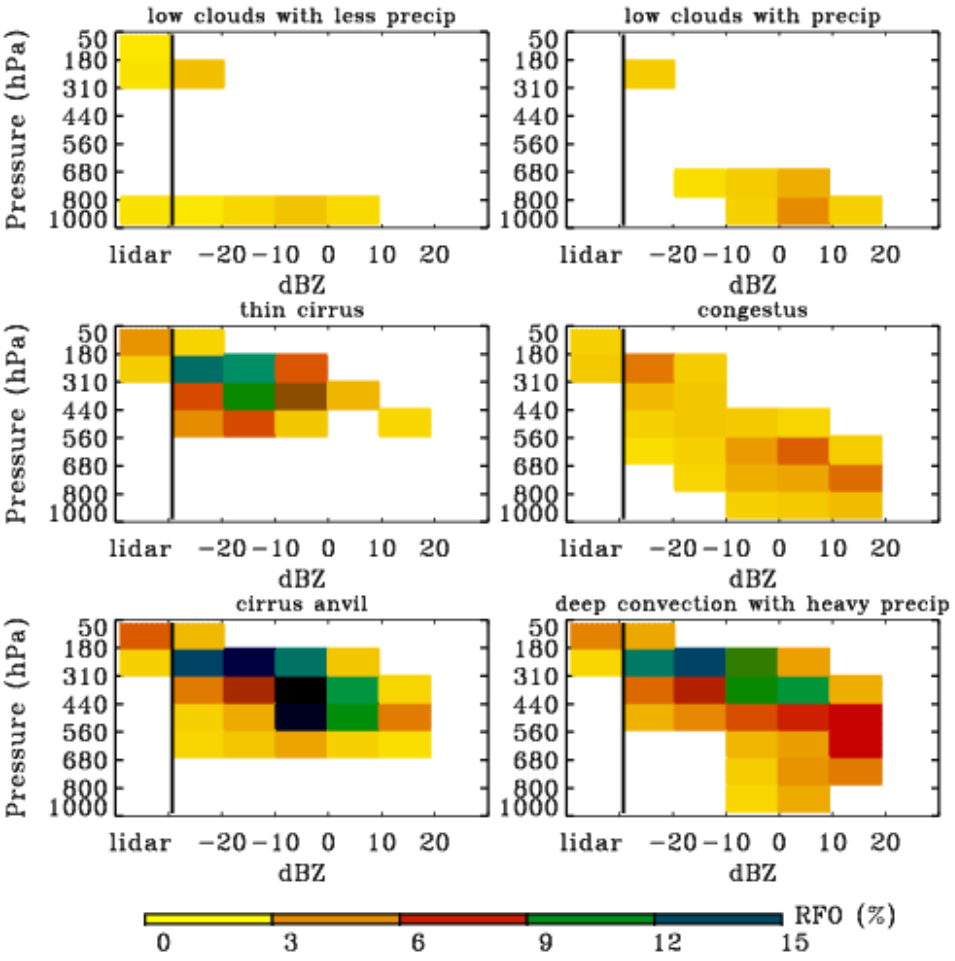

Figure 5. Joint histograms of cluster centroids from CAM3.1 by assigning cloud simulations into observational clusters based on the minimum Euclidean distance.

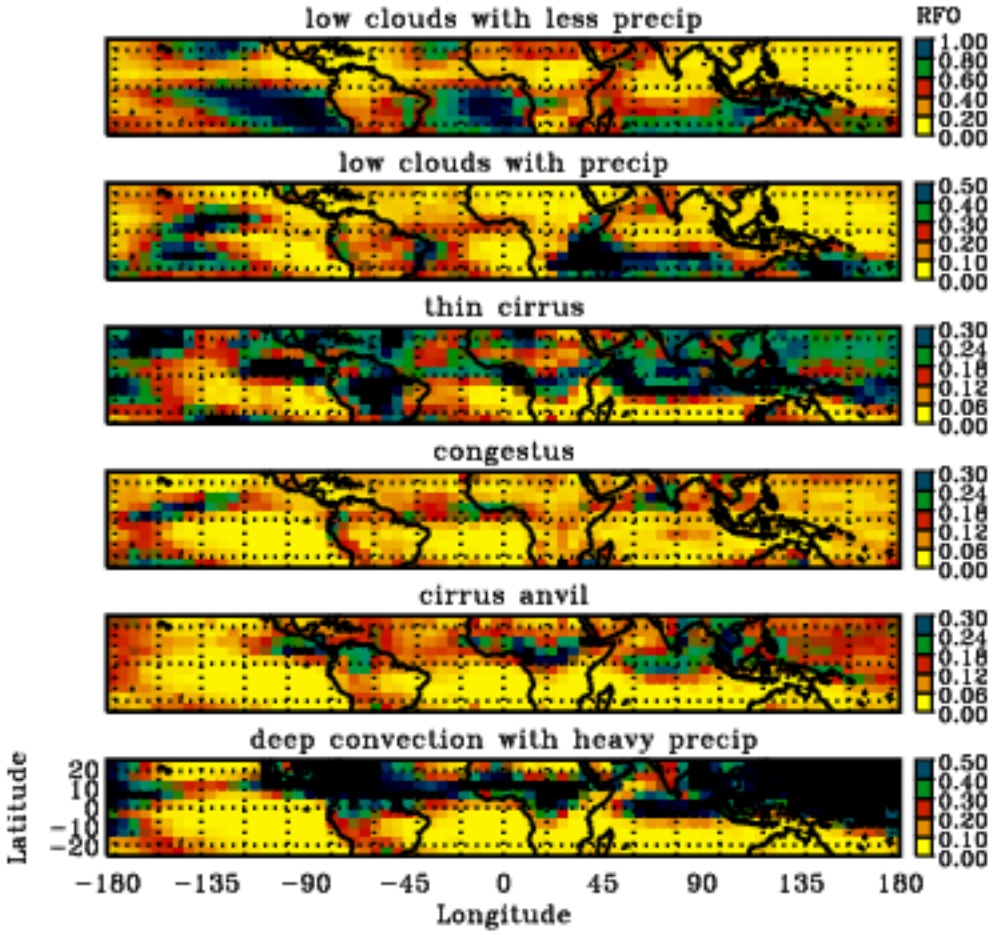

Figure 6. The temporal-averaged occurrence fraction of each cluster from cloud simulations in CAM3.1 forecasts.

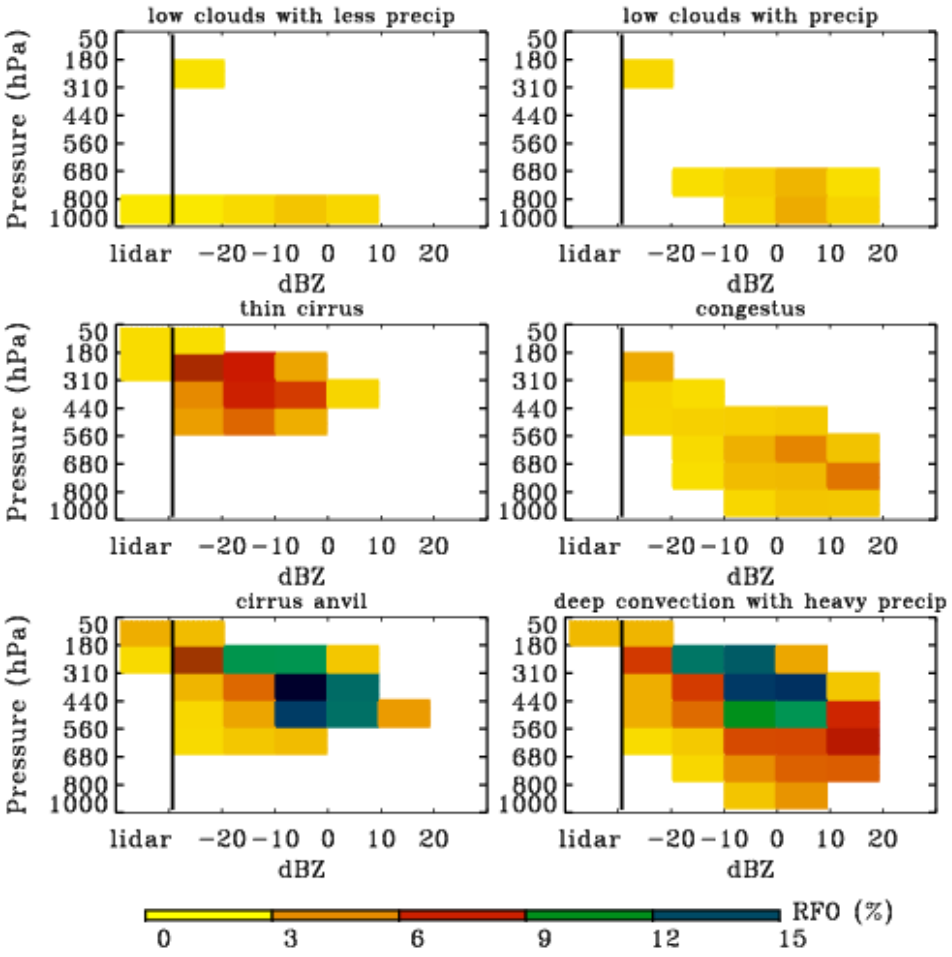

Figure 7. As in Fig. 5 but from CAM3.5.

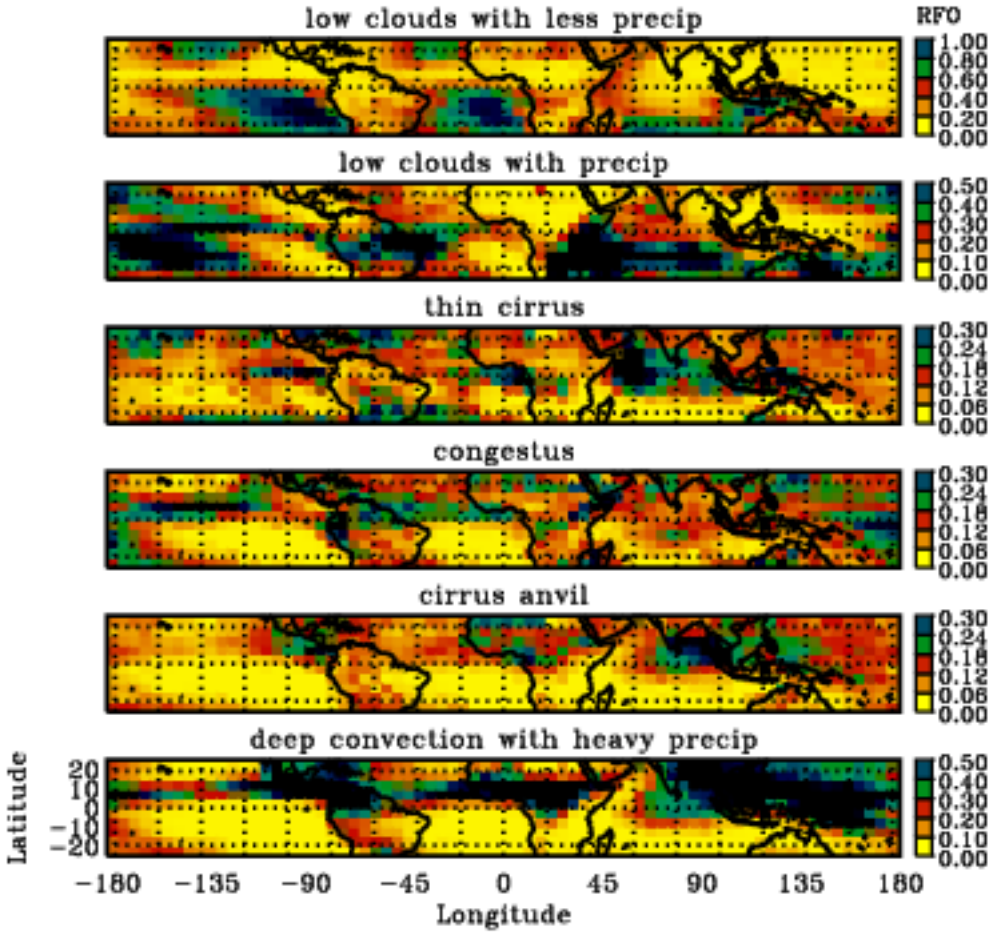

Figure 8. As in Fig. 6 but from CAM3.5.

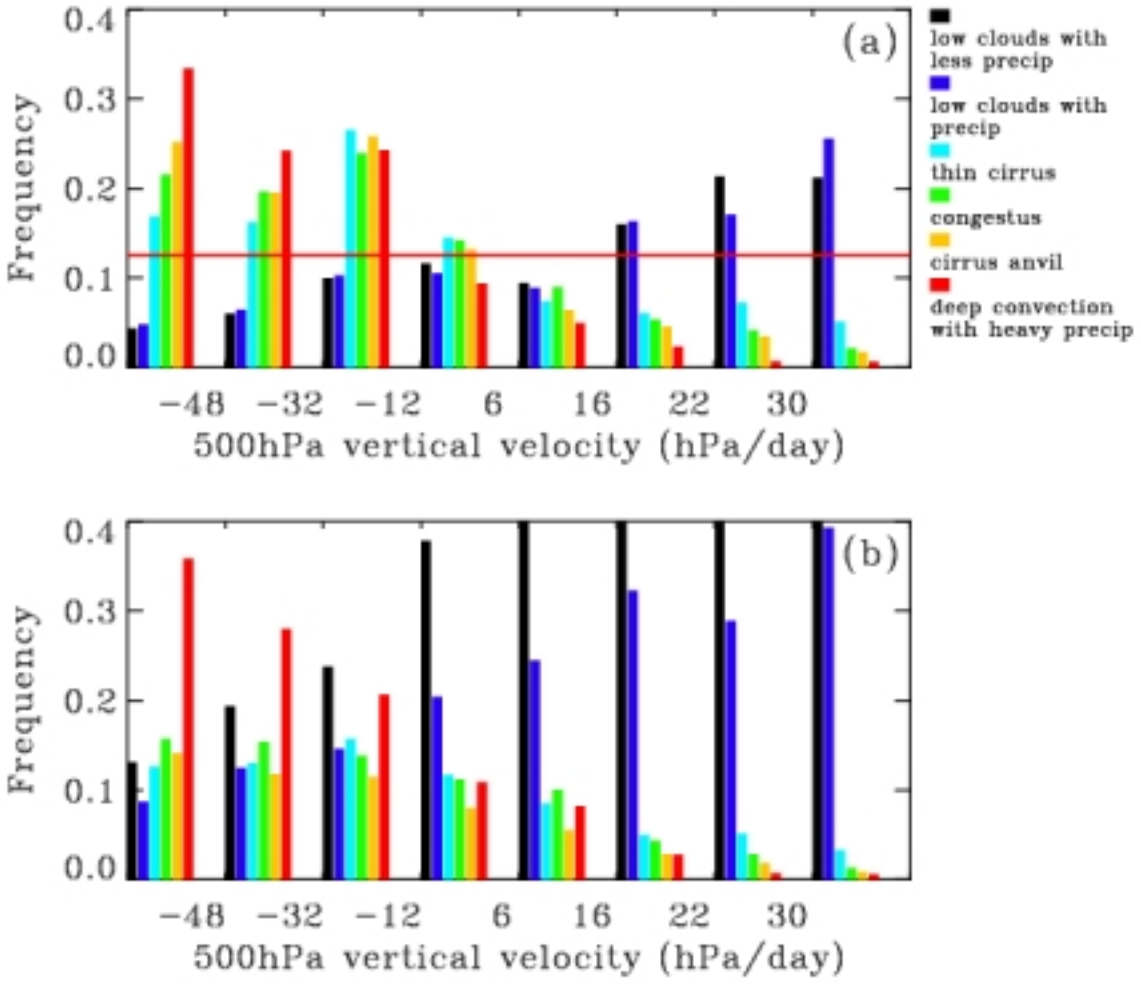

Figure 9. The frequency of the occurrence for each cluster from CloudSat-CALIPSO observation as a function of large-scale dynamics defined by the monthly mean vertical velocity at 500hPa calculated using NCEP analysis data. The boundaries for each omega bin are determined such that each bin represents the equivalent occurrence frequency of vertical velocities. (a) The fraction of elements of a given cluster which occur in the given vertical velocity bin. For this measure, the sum of the frequencies in the eight vertical velocity bins for each cluster is 1. The red line indicates the occurrence frequency if there were no association of cloud clusters with the 500hPa vertical velocity. (b) The fraction of cloudy elements of a given vertical velocity bin which belong to a given cluster. For this measure, the sum of the frequencies of the six clusters in each vertical velocity bin is 1.

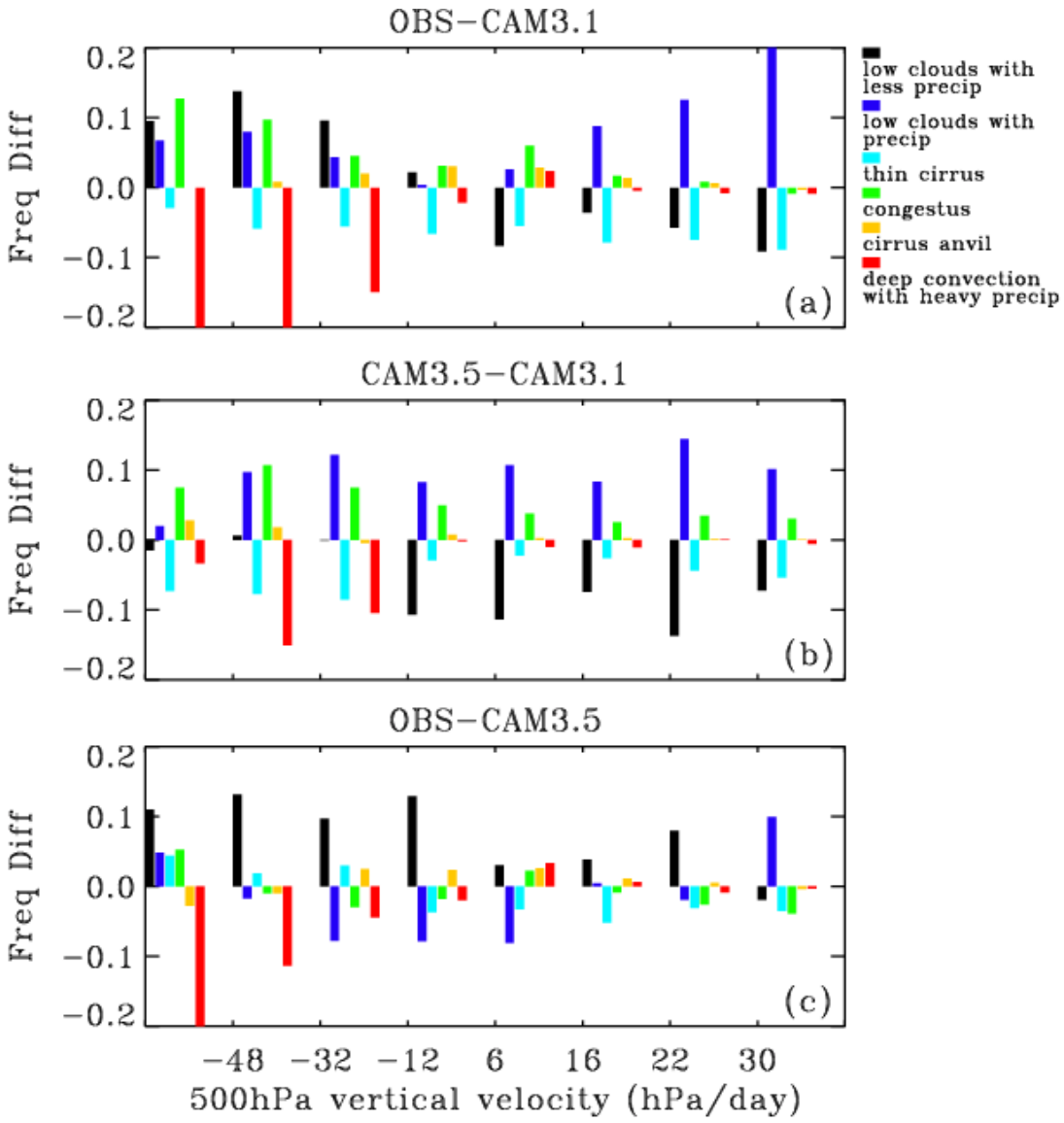

Figure 10. The frequency difference of the six clusters in each vertical velocity bin for the fraction of elements of a given vertical velocity bin which belong to a given cluster. This measure is the same as was displayed in Figure 9(b): (a) The difference between observations and CAM3.1forecasts, (b) the difference between CAM3.5 and CAM3.1, and (c) the difference between observations and CAM3.5.

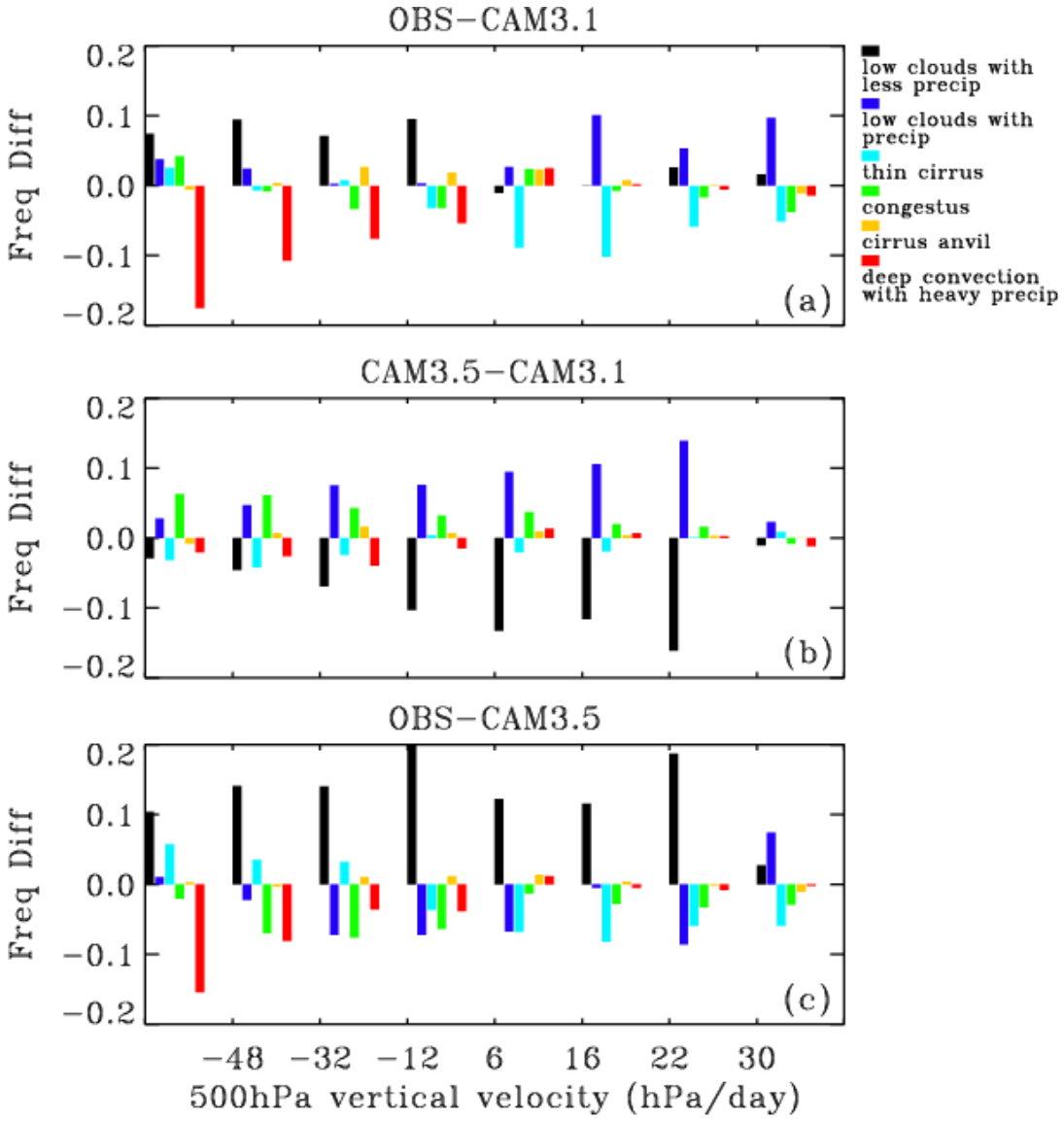

Figure 11. As in Fig. 10 but for CAM3 climate integrations.